A High-Accuracy Rainfall Dataset by Merging Multi-Satellites and Dense Gauges over Southern Tibetan Plateau for 2014-2019 Warm Seasons

Kunbiao Li[1], Fuqiang Tian[1], Mohd Yawar Ali Khan[2], Ran Xu[1], Zhihua He[3], Long Yang[4], Hui Lu[5], Yingzhao Ma[6]

[1] Department of Hydraulic Engineering, Tsinghua University, Beijing, China

[2] Department of Hydrogeology, King Abdul-Aziz University, Jeddah, Saudi Arabia

[3] Centre for Hydrology, University of Saskatchewan, Saskatoon, SK S7N 5C8, Canada

[4] School of Geography and Ocean Science, Nanjing University, Nanjing, China

[5] Department of Earth System Science, Tsinghua University, Beijing, China

[6] Cooperative Institute for Research in the Atmosphere, Colorado State University, 1375 Campus Delivery, Fort Collins, CO 80523, United States.

Correspondence: Fuqiang Tian (tianfq@mail.tsinghua.edu.cn)

Abstract

Tibetan Plateau (TP) is well known as the Asia's water tower from where many large rivers originate. However, due to complex spatial variability of climate and topography, there is still a lack of high-quality rainfall dataset for hydrological modelling and flood prediction. This study, therefore, aims to establish a high-accuracy daily rainfall product through merging rainfall estimates from three satellites, i.e., GPM-IMERG, GSMaP, and CMORPH, based on the likelihood measurements of a high-density rainfall gauge network. The new merged daily rainfall dataset with a spatial resolution of 0.1°, focuses on warm seasons (June 10th - October 31st) from 2014 to 2019. Statistical evaluation indicated that the new dataset outperforms the raw satellite estimates, especially in terms of rainfall accumulation and the detection of ground-based rainfall events. Hydrological evaluation in the Yarlung Zangbo River Basin demonstrated high performance of the merged rainfall dataset in providing accurate and robust forcings for streamflow simulations. The new rainfall dataset additionally shows superiority to several other products of similar types, including MSWEP and CHIRPS. This new rainfall dataset is publicly accessible at https://doi.org/10.11888/Hydro.tpdc.271303 (Li et al.,2021).

1. Introduction

Precipitation, linking atmospheric and hydrological processes, serves as a crucial component of the water cycle (Eltahir & Bras, 1996; Trenberth et al., 2003). Gridded precipitation datasets become more and more popular with the advent of satellite precipitation measurement. Most famous satellite gridded precipitation datasets include Tropical Rainfall Measuring Mission (TRMM) (Huffman et al., 2007) and its successor the Integrated Multi-satellite Retrievals for Global Precipitation Measurement mission (GPM-IMERG) (Hou et al., 2014), the Global Satellite Mapping of Precipitation

42 (GSMaP) (Ushio et al., 2009), the Climate Prediction Centre (CPC) MORPHing

43 technique (CMORPH) (Joyce et al., 2004), etc. These products have been successfully

44 applied in various hydrometeorological studies and water resources management

45 practices (Kidd, C., & Levizzani, V., 2011; Jiang et al., 2012; Tong et al., 2014; Yang et

46 al., 2015; Sun et al., 2016; Wang et al., 2017).

47 However, all existing precipitation datasets show insufficient accuracy in high

48 mountainous regions (Yilmaz et al., 2016; Derin et al., 2018; Derin et al., 2019;

49 Anagnostou & Zhang, 2019), which hinders our understanding of climate and

50 hydrological processes over these areas. This can be attributed to the complex physical

51 nature of electromagnetic transmission and precipitation forming processes (Hong et

52 al., 2007; Bitew & Gebremichael 2010; Dinku et al., 2010), and harsh environments in

53 high mountains that lead to very limited deployment of in-situ rain gauges with

54 insufficient representation of ground observations for training satellite-based

55 precipitation retrieval algorithms. For instance, the Tibetan Plateau (TP) as the roof of

56 the world is surrounded by imposing mountain ranges with an average elevation

57 exceeding 4000 m. It generates several large rivers in Asia and provides invaluable

58 freshwater resources for more than 1.4 billion people living downstream (Immerzeel et

59 al., 2010). However, this vast plateau has very limited number of precipitation gauges

60 across its 2.5 million km^2 area. The precipitation gauge network operated by China

61 Meteorological Agency (CMA) contains only 86 gauges over the entire TP (Figure 1).

62 These gauges are essential to correct satellite precipitation datasets. For example, GPM-

63 IMERG 'Final' Run dataset uses Global Precipitation Climatology Centre (GPCC)

64 database, GSMap_Gauge and CMORPH use NOAA Climate Prediction Centre (CPC)

65 database. Although both GPCC and CPC databases received data through Global

66 Telecommunication System (GTS), only part of the above-mentioned gauges in TP

67 were utilized (Xie et al., 2007; Becker 2013). Previous evaluations over the TP

68 indicated that most products present dependence on topography to varying degrees, and

69 products adjusted by gauge observations shows better performance than satellite-only

70   products (Gao et al.,2013; Lu et al., 2018). Therefore, a better spatial coverage of rain

71   gauges is critical to correct satellite products in high mountains.

72   In 2014, the Ministry of Water Resources of China (MWR) launched the flash

73   flood monitoring and alarming campaign. A large number of rain gauges is now

74   accessible over the TP, especially in the southern TP. There are 440 new rain gauges

75   totally involved in 6 years, and are available since 2014, independent of the existing

76   CMA precipitation gauge network (Figure 1). These gauges provide measurements of

77   precipitation in liquid phase (i.e., rainfall) at event time scale. A couple of recent studies

78   have demonstrated the utility of this rain gauge network (Xu et al., 2017; He et al., 2017;

79   Tian et al., 2018; Wang et al., 2020). For instance, Xu et al. (2017) evaluated the

80   performance of TRMM and GPM and the dependence on topography and rainfall

81   intensity based on the network. Their results demonstrated that the data quality of this

82   dense gauge network is strictly controlled, serving as the currently highest gauge dense

83   for satellite product evaluation on TP. Wang et al. (2020) used the gauge data to validate

84   their reproduced precipitation dataset. However, there is not a merging product that

85   assimilate the observations from this dense rain gauge network. This is apparently a

86   unique opportunity to improve the performance of existing satellite-based precipitation

87   datasets for its highest density and quality.

88   This study aims to provide a high-accuracy rainfall dataset by merging all

89   available ground gauges and three good-quality satellite precipitation datasets over the

90   southern TP for the warm seasons (June 10th - October 31st) from 2014 to 2019. The

91   remainder of this paper is organized as follows: Section 2 describes the study area and

92   the source data. Section 3 provides details of the data merging method and the methods

93   adopted to evaluate the quality of dataset. Results are presented in Section 4. The data

94   availability and summary are provided in Section 5 and Section 6, respectively.

2. Study Area and Source Data

2.1. Southern Tibetan Plateau

Tibetan Plateau, known as the Asian water tower, mainly covers parts of China, India, Myanmar, Bhutan, Nepal and Pakistan. ~~Tibetan Plateau, known as the Asian water tower, borders India, Myanmar, Bhutan and Nepal to the south and Pakistan to the west.~~ Various climate systems affect the plateau, including westerly winds in winter and the Indian monsoon in summer (Yao et al., 2012). Many Asian large rivers originate from this vast area, including the Yellow River, the Yangtze River, the Yarlung Zangbo River (YZR), Jinsha River (JR), Lancang River (LR), Salwen River (SR), Irrawaddy River (IR), Ganges River (GR), and Indus River (IDR). This study is focused on the southern part of TP (Figure 1), including the upper YZR Basin (YZRB) as a major basin.
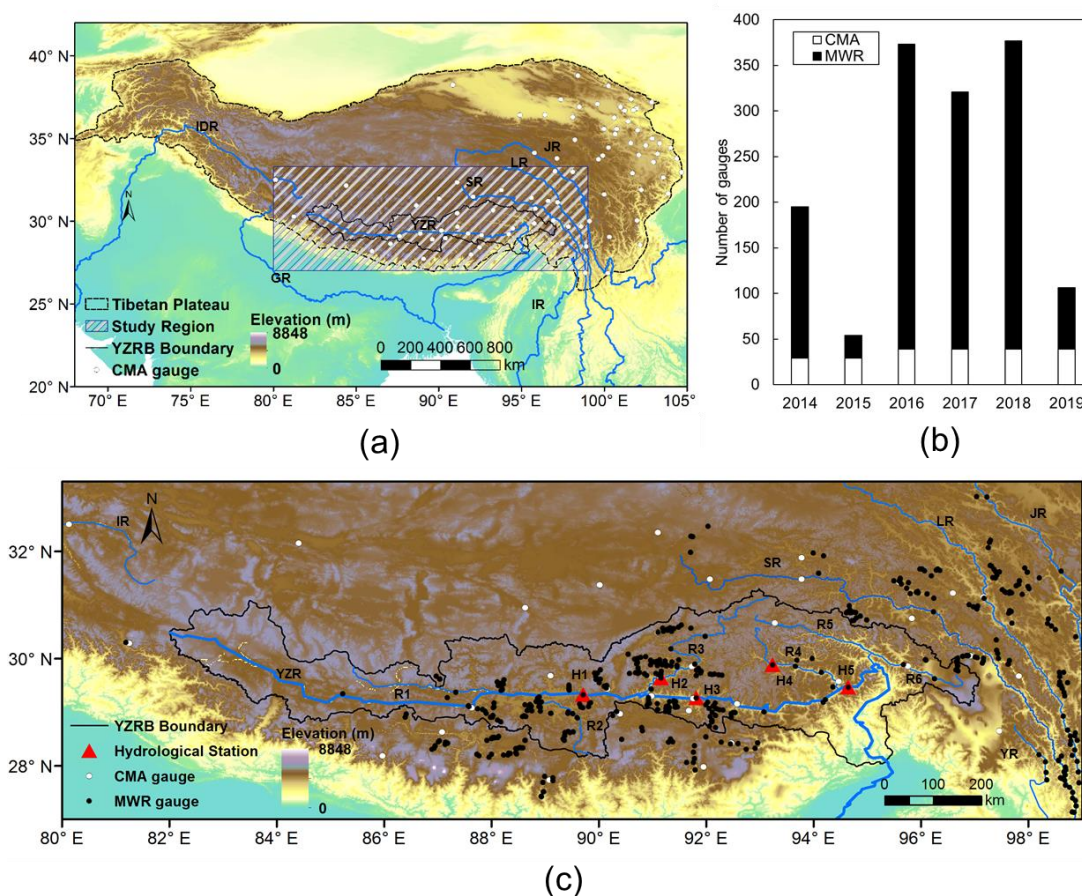
Figure 1. (a) The location and topography of the TP and the spatial distributions of CMA gauges.

108 (b) Numbers of ground gauges installed by CMA and MWR in southern TP during 2014-2019, (c)

109 Locations of CMA and MWR rain gauges and main hydrological stations in southern TP. The names

110 of hydrological stations are labelled as H1-Yangcun, H2-Lhasa, H3-Nugesha, H4-Gongbujiangda,

111 H5-Nuxia. The names of tributary rivers are labelled as R1-Duoxiong Zangbo, R2-Nianchu River,

112 R3-Lhasa River, R4-Niyang River, R5-Yigong Zangbo, R6-Parlung Zangbo.

2.2. Ground gauged rainfall

114 We combined two rain gauge networks managed by MWR and CMA to obtain a

115 high-quality ground reference dataset up to date. The number of rain gauge is presented

116 in Figure 1b, and varies across different years. The spatial distribution of all gauges is

117 presented in Figure 1c. The gauges are mainly located in the middle reaches of YZRB

118 and the east part of the study area. Despite the high density, we can see these rain gauges

119 are not evenly distributed across the space. This makes satellite rainfall products over

120 varying altitudes and aspects important. Daily rainfall observations during the warm

121 seasons of 2014-2019 were accumulated from the original event scale measurements.

122 Total number of the CMA and MWR gauges ranges from 53 in 2015 to 377 in 2018,

123 forming the densest rain gauge network up till now.

124 The CMA gauge data has been widely demonstrated as reliable and accurate in

125 previous studies (Zhai et al., 2005; Su et al., 2020; He et al., 2020). Gauge data used in

126 this study has been manufactured under strict quality control procedures, including (1)

127 internal consistency check, (2) extreme values check (0~85mm/h), and (3) spatial

128 consistency check (Ren et al., 2010). Rain gauges with erroneous values (e.g.

129 enormously large values) were discarded from the entire records. Through strict quality

130 control methods, the warm seasons from June 10th to October 31st were selected as the

131 study period to maintain the high quality of outcome rainfall dataset.

2.3. Satellite Precipitation Datasets

133 Three satellite precipitation products were chosen for the data merging procedure

134 (Lu et al., 2019; Derin et al., 2019; Tang et al., 2020), including GPM-IMERG 'Final'

135 run (here after referred to as IMERG) from the National Aeronautics and Space

136 Administration (NASA) (https://disc.gsfc.nasa.gov/), the GSMaP_Gauge (here after

137 referred to as GSMaP) from Japan Aerospace Exploration Agency (JAXA)

138 (http://sharaku.eorc.jaxa.jp) and the CMORPH v1.0 from NOAA CPC

139 (ftp://ftp.cpc.ncep.noaa.gov/precip/CMORPH_V1.0/). Spatial resolutions and temporal

140 frequency of the satellite datasets are listed in Table 1. To be consistent, IMERG and

141 GSMaP data were accumulated to daily scale (08:00-08:00 of local time, i.e. UTC+8)

142 and CMORPH was bilinearly interpolated to the grid resolution of 0.1°.

143   The merged dataset was further compared with two popular merged rainfall

144 datasets of Climate Hazards Group InfraRed Precipitation with Stations (CHIRPS)

145 (Funk et al., 2015) and Multi-Source Weighted-Ensemble Precipitation (MSWEP)

146 (Beck et al., 2019). CHIRPS was originated by merging CHPClim, thermal infrared,

147 TRMM3B42, NOAA CFSv2 precipitation data, and ground observation precipitation

148 data. MSWEP was merged from multiple datasets including CPC, GPCC, CMORPH,

149 GSMaP-MVK, GPM-IMERG, ERA5, and JRA-55. CHIRPS and MSWEP showed

150 great potentials in rainfall estimates in previous studies (Liu et al., 2019).

151   Table 1. Multiple satellite precipitation datasets used in this study.

Datasets	Resolution	Frequency	Source	Reference
GPM IMERG	0.1 °x 0.1 °	0.5 hourly	NASA	(Hou et al., 2014)
GSMaP_Gauge	0.1 °x 0.1 °	1 hourly	JAXA	(Ushio et al., 2009)
CMORPH v1.0	0.25 °x 0.25 °	daily	CPC	(Joyce et al., 2004)
CHIRPS v2.0	0.25 °x 0.25 °	daily	USGS and CHC	(Funk et al., 2015)
MSWEP v2	0.1 °x 0.1 °	3 hourly	-	(Beck et al., 2019)

152 **3. Methodology**

153   We used the Dynamic Bayesian Model Averaging (DBMA) method (Ma et al.,

154 2017) to merge the satellite datasets with in-situ rain gauges. To evaluate the quality of

155 the new dataset, we carried out statistical and hydrological evaluations and comparisons

156 with CHIRPS and MSWEP in southern TP.

157 **3.1. Dynamic Bayesian Model Averaging method**

158 The Dynamic Bayesian Model Averaging (DBMA) method developed by Ma et

159 al. (2018) was utilized in this work. A flow chart of the merging method is shown in

160 Figure 2. In the first step, a training dataset was formed by selecting samples from the

161 ground gauged data and three original satellite datasets. The training period was set as

162 40 days. Increasing the length of the training period did not lead to obvious

163 improvement of the merging method (Ma et al., 2018). In the second step, the training

164 dataset was transformed by the Box-Cox Gaussian distribution, and the optimal weights

165 for each of the original satellite datasets on a specific grid where a ground gauge is

166 located on each training day were estimated by a logarithmic likelihood equation and

167 the optimal expectation algorithm. In the third step, an ordinary Kriging interpolation

168 method was applied to spatially interpolate the daily weights onto grids with no gauges.

169 Finally, posterior spatiotemporal weights were used to obtain the final merged rainfall

170 dataset. The DBMA-merged data has been proved in Ma et al. (2017) to outperform

171 original satellite data during 2007-2012 over TP.

172
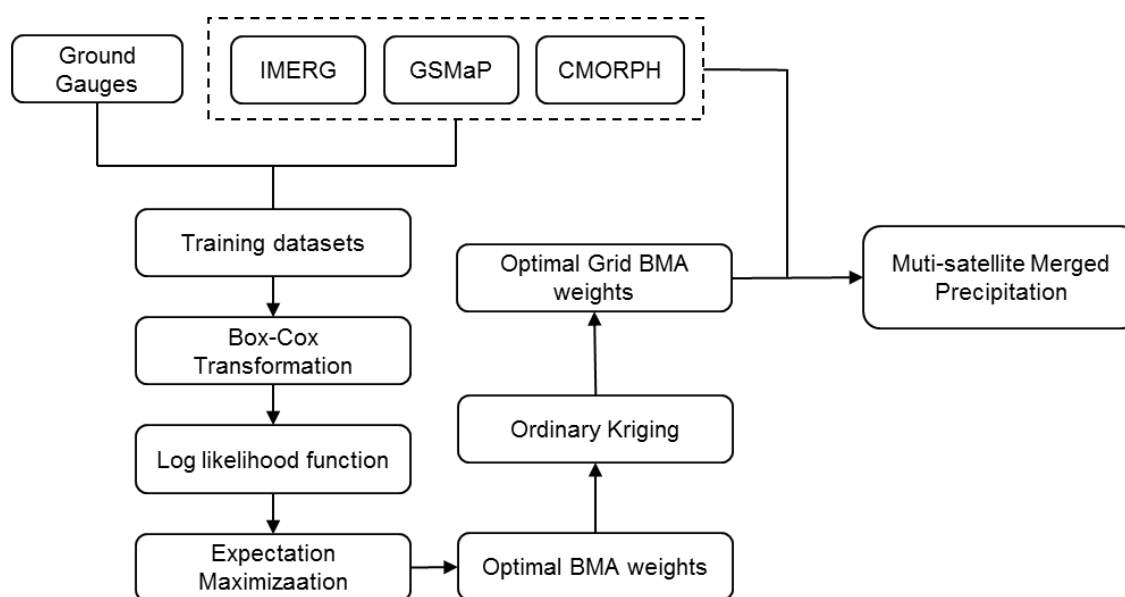
173 Figure 2. Flowchart of the DBMA merging method (adapted from Ma et al., 2018).

174   For statistical evaluation of the merged data against ground gauges, around 85%

175 of the gauges were randomly selected to form a training gauge set for the merging

176 approach in each year during 2014-2019, and the remaining 15% were used for test.

177 Training method DBMA of 40 days was only conducted in training dataset. Table 2 lists

178 the numbers of training and test gauges in each of the warm seasons. The spatial

179 distributions of gauges in each year are presented in Figure S1. Data from all gauges

180 were involved in the training procedure of the final released version of the merged data.

181   Table 2. Number of rain gauges for training and test in 2014-2019.

Year	Total number of rain gauges	Number of training gauges	Number of test gauges
2014	195	166	29
2015	54	46	8
2016	373	317	56
2017	321	273	48
2018	377	320	57
2019	106	90	16

182 **3.2. Statistical Evaluation**

183   Performance of the multiple datasets were statistically evaluated by comparing

184 with ground observations on the corresponding statelite grids. Relative bias (RB) and

185 normalized root mean square error (RMSE) were adopted to measure the amount

186 difference between the gridded rainfall and the gauged rainfall. Correlation Coefficient

187 (CC) was used to evaluate the consistency between satellite estimates and gauge

188 observations. The skill of rainfall data on detecting rainfall occurrence (rainfall events

189 higher than zero) was evaluated through a set of metrics (similarly to Wilks, 2006): i.e.

190 the probability of detection (POD) assessing how good the multiple rainfall datasets are

191 at detecting the occurrence of rainfall, false alarm ratio (FAR) measuring how often the

192 gridded rainfall datasets detect rainfall when there actually is not rainfall, and critical

193 success index (CSI) measuring the ratio of rainfall events that are correctly detected by

194 the gridded datasets to the total number of observed or detected events. Equations for

195   the above metrics are shown in Table 3.

196   Table 3. Statistical indices that were used to assess the performance of the gridded rainfall

197   datasets.

Statistical Indicators	Equation	Optimal Value	Equation number
Relative Bias (RB)	$Bias = \dfrac{\sum_{i=1}^{n}(S_i - G_i)}{\sum_{i=1}^{n} G_i}$	0	(1)
Correlation Coefficient (CC)	$CC = \dfrac{[\sum_{i=1}^{n}(S_i - \bar{S}) \cdot (G_i - \bar{G})]^2}{\sum_{i=1}^{n}(S_i - \bar{S})^2 \cdot \sum_{i=1}^{n}(G_i - \bar{G})^2}$	1	(2)
Root Mean Square Error (RMSE)	$RMSE = \sqrt{\dfrac{1}{n}\sum_{i=1}^{n}(S_i - G_i)^2}$	0	(3)
Probability of Detection (POD)	$POD = \dfrac{a}{a + c}$	1	(4)
False Alarm Ratio (FAR)	$FAR = \dfrac{b}{a + b}$	0	(5)
Critical success index (CSI)	$CSI = \dfrac{a}{a + b + c}$	1	(6)

198   For the equations listed in Table 3, n is the total number of gridded product data

199   and gauge observation data; i is the ith of satellite product data and gauge

200   observation data; G_i means gauge observation and $\bar{G}$ is the average of gauge

201   observation. S_i and $\bar{S}$ are gridded estimates and their average, respectively. a

202   represents hit (i.e., event was detected to occur and observed to occur), b represents

203   false alarm (i.e., event was detected to occur but not observed to occur), and c

204   represents miss (i.e., event was not detected to occur but observed to occur).

205   Triple Collocation (TC) technique provides a platform for quantifying the root

206   mean square errors of three products that estimate the same geophysical variable

207   (Stoffelen, 1998). Roebeling et al. (2012) successfully applied the TC technique to

208   estimate errors of three rainfall products across Europe. An extended Triple Collocation

209   (ETC) introduced in Kaighin et al. (2014), which is able to estimate errors and

210   correlation coefficients with respect to an unknown target was used in this study to

211 compare the performance of the DBMA-merged data and two previous merged datasets

212 of CHIRPS and MSWEP.

213 **3.3. Hydrological Evaluation**

214   In addition to the statistical assessments against rain gauges, hydrological

215 assessment was used as a tool to test the performance of merged rainfall datasets on

216 forcing hydrological modelling in the study area (similarly see Yong et al, 2012; Xue

217 et al, 2013; Yong et al, 2014; Li et al, 2014). In this section, a semi-distributed

218 hydrological model developed by Tian (2006), namely Tsinghua Hydrological Model

219 based on Representative Elementary Watershed (THREW), was adopted for the

220 hydrological assessment of rainfall datasets in the YZRB. YZRB has a drainage area of

221 approximately 240,480 km^2 within China's boarder. The basin elevation ranges from

222 143 to 7,261 m, with an average of around 4,600 m. YZR is one of the most important

223 transboundary rivers in South Asia and the highest river in the world, which is

224 characterized by a dynamic fluvial regime with exceptional physiographic setting

225 spreading along the eastern Himalayan region (Goswami, 1985). Due to complex

226 terrain and strongly varying elevation, the YZRB is under control of a variety of climate

227 systems, such as the semi-arid plateau climate prevailing in the upper and middle

228 reaches, and the mountainous subtropical and tropical climates prevailing in the lower

229 reaches. In the cold upper reaches, the mean annual rainfall is less than 300 mm. In the

230 warm middle reaches, the mean annual rainfall falls between 300 mm and 600 mm.

231   The whole basin area above the Nuxia hydrological station was divided into 63

232 Representative Elementary Watersheds (REWs). Model parameters were calibrated by

233 daily discharges measured at the Nuxia station. The calibration period is scheduled to

234 run in the warm seasons from June 10th to October 31st in 2014- 2017, encompassing a

235 period length of 576 days. The validation period includes two warm seasons in 2018

236 and 2019 with a total duration of 288 days. Descriptions of the calibrated model

237 parameters can be found in Table 4. An automatic algorithm pySOT developed by D.

238 Eriksson et al (2019) was used to optimize the parameter values based on an objective-

239 function of *NSE* (Nash and Sutcliffe, 1970) in Eq. 7. To conduct a continuous

240 hydrological simulation in the study period, the datasets of daily grid-based

241 precipitation over China (Zhao et al., 2014) were used as model inputs in the non-warm

242 seasons when merged rainfall is not available.

243 Table 4. Calibrated parameters of the THREW model.

Symbol	Description	Unit	Value Range
kv	Fraction of potential transpiration rate over potential evaporation	-	0.001-0.8
n^t	Manning roughness coefficient for hillslope	-	0.0001-0.2
GaIFL	Spatial heterogeneous coefficient for infiltration capacity	-	0.0001-0.7
GaEFL	Spatial heterogeneous coefficient for exfiltration capacity	-	0.0001-0.7
GaETL	Spatial heterogeneous coefficient for evapotranspiration capacity	-	0.0001-0.7
WM	Tensor water storage capacity	cm	0.1-10
B	Shape coefficient to calculate the saturation excess runoff area	-	0.01-1
Gaus	Coefficient representing spatial heterogeneity of exchange term between t-zone and r-zone	-	0.001-10
KKA	Exponential coefficient to calculate subsurface flow	-	0.01-6
KKD	Linear coefficient to calculate subsurface flow	-	0.001-0.5
MM	Snow melting degree-day factor	mm/day	0.001-10
MMG	Ice melting degree-day factor	mm/day	0.001-10
C1+C2	Muskingum parameter	-	0.0001-1
C1/(C1+C2)	Muskingum parameter	-	0.0001-1

$$NSE = 1 - \frac{\sum_{n=1}^{N}(Q_{obs}^n - Q_{sim}^n)^2}{\sum_{n=1}^{N}(Q_{obs}^n - \bar{Q}_{obs}^n)^2} \tag{7}$$

244 where, N is the total number of days in the evaluation period, Q_{obs}^n and Q_{sim}^n

245 represent the observed and simulated runoff on the nth day, respectively. $\bar{Q}_{obs}$

246 represents the average of observed runoff in the evaluation period.

4. Results and Discussions

4.1. Spatiotemporal Patterns

Based on the merging method, a new daily rainfall dataset with spatial resolution of 0.1°×0.1° in the warm seasons from June 10th to October 31st (144 days in each year) in 2014-2019 (864 days in six years) was generated. Figure 3 presents the spatial pattern of the mean rainfall over the six warm seasons of the merged data in southern TP. It is shown that extremely high summer rainfall centres concentrate in the south-eastern and south-western of the study area where is known as a world-famous heavy rainfall centre (see Biskop et al., 2015; Bookhagen & Burbank, 2006; Kumar et al., 2010).
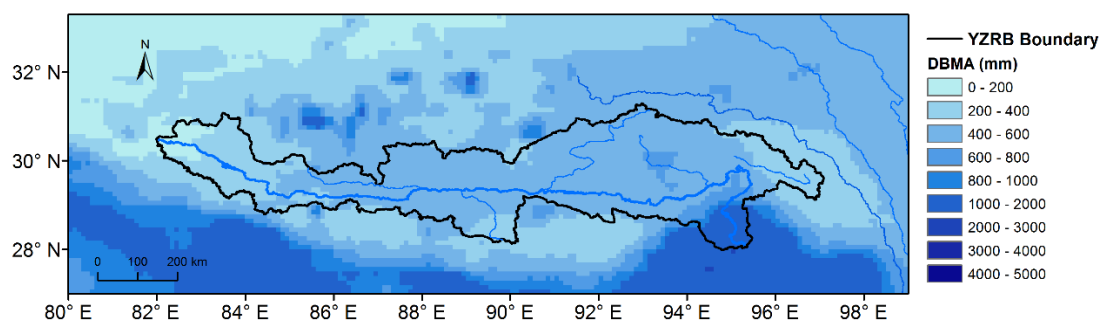
Figure 3. Spatial pattern of mean rainfall over six warm seasons in 2014-2019 of the DBMA-merged data in southern TP.

In addition, Figure 4 compares the time series of average daily weight and rainfall over the YZRB basin derived from the DBMA-merged data and the original satellite datasets. As expected, the DBMA-merged daily rainfall in general fall in the envelope ranges of the three satellite datasets. Merged data is closer to CMORPH in June, September and October, while showing equal closeness to all the three source satellite data in July and August. It indicates that CMORPH is closer to the in-situ gauges than IMERG at basin scale when rainfall value is small, especially for light rainfall events smaller than 2 mm, but this difference tends to be small for heavy rainfall events.

267
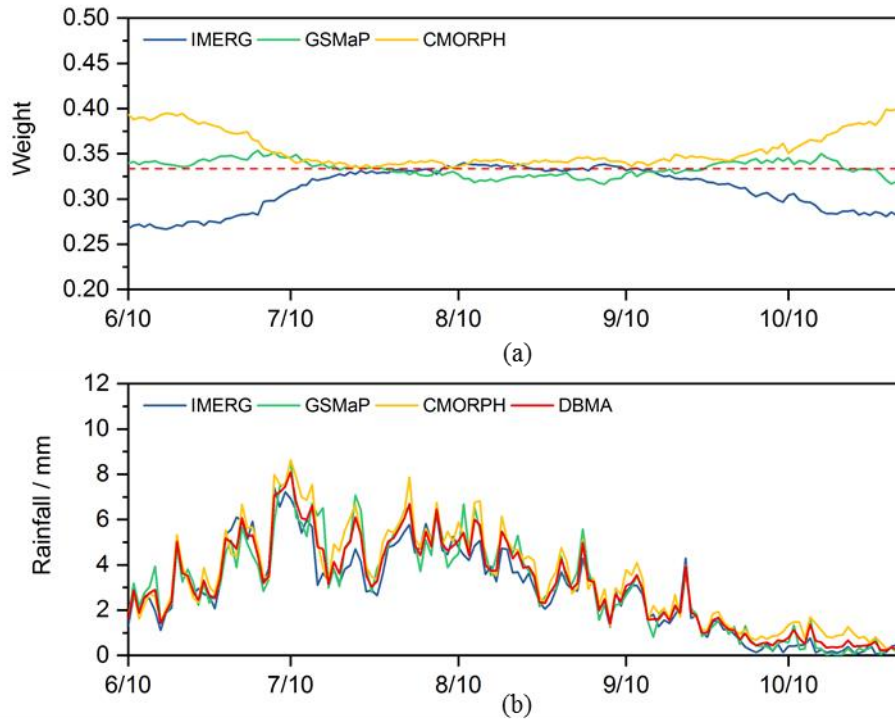
268   Figure 4. Seasonal variations in basin-averaged (a) weights and (b) rainfall estimates of the

269   multiyear daily values of IMERG, GSMaP, CMORPH and DBMA.

270 **4.2. Statistical Evaluation**

271   Figure 5 shows the statistical evaluation of the merged and original datasets in the

272 warm seasons. The statistical indices were calculated for three gauge groups including

273 the training gauges, the test gauges and all gauges at different elevation bands. The

274 datasets in general presented comparable performance for the training and test gauge

275 groups, indicating that the sampling procedure of ground gauges is adequately random.

276 The comparable performance of merged data in training and test gauge groups

277 demonstrated robustness of the merging method on varying gauges. In terms of RSME,

278 CC, and POD, the DBMA-merged data shows much better performance on all gauge

279 groups and elevation bands than the original satellite datasets. The smallest RSME of

280 merged data indicate that the total rainfall amount of the merged data during the

281 evaluation period showed the lowest difference from the total amount of gauged rainfall.

282 The highest CC and POD highlight the best consistency between merged data and

283   ground gauge data on days when most regions in the basin were rainy. The RB of

284   DBMA-merged data is at an intermediate level among the satellite datasets as it is the

285   weighted average of those three datasets. The higher FAR and lower CSI of DBMA-

286   merged data could be attributed to that the merging method detected rainfall events

287   when rainfall estimate is higher than zero in any one of the three satellite datasets and

288   thus resulted in overestimated rainfall occurrence. The overestimated rainfall

289   occurrence might have small effects on the estimation of rainfall amount, as most of

290   the falsely alarmed events were tiny. It is noteworthy that the performance of the

291   merged data shows smaller variance across elevation bands than that of the original

292   satellite datasets. This is most likely benefiting from the spatially dynamic optimal

293   weights for the original satellite data. However, the merged data presented the largest

294   difference from gauged data at the altitudes of 3000-3500 m, because there are much

295   less gauges on this elevation zone.

296
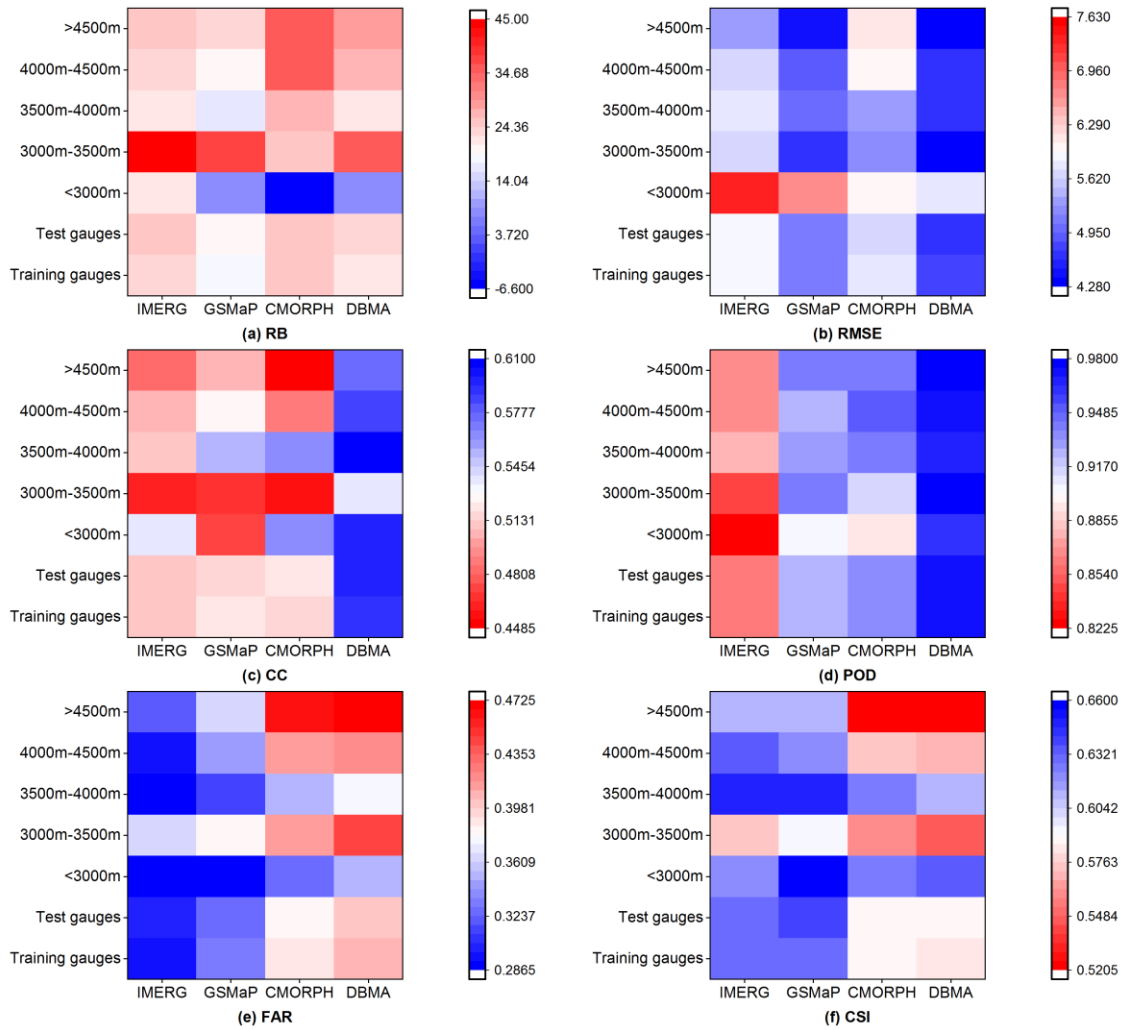
297 Figure 5. Comparisons of the statistical indices of (a) RB, (b)RMSE, (c) CC, (d) POD, (e) FAR

298 and (f) CSI for training gauges, test gauges and all gauges at five elevation bands.

299 Figure 6 shows CC of different datasets on specific gauges. The merged data

300 presents higher CC values in regions where are densely gauged, i.e., the middle reaches

301 of YZRB and the east part of the study region, which can be expected as the dense

302 ground gauges provided strongly informative benchmark likelihoods for the estimation

303 of satellite data weights. On most of the gauges (Figure 6a), the merged-data presented

304 higher CC values than the IMERG data, which is consistent with Figure 5c. On contrary,

305 the merged-data showed reduced CC than GSMaP and CMORPH on more gauges

306 (Figures 6b-c), indicating that involving IMERG data in the merging procedure on these

307 gauges lead to deteriorated consistence performance.

308
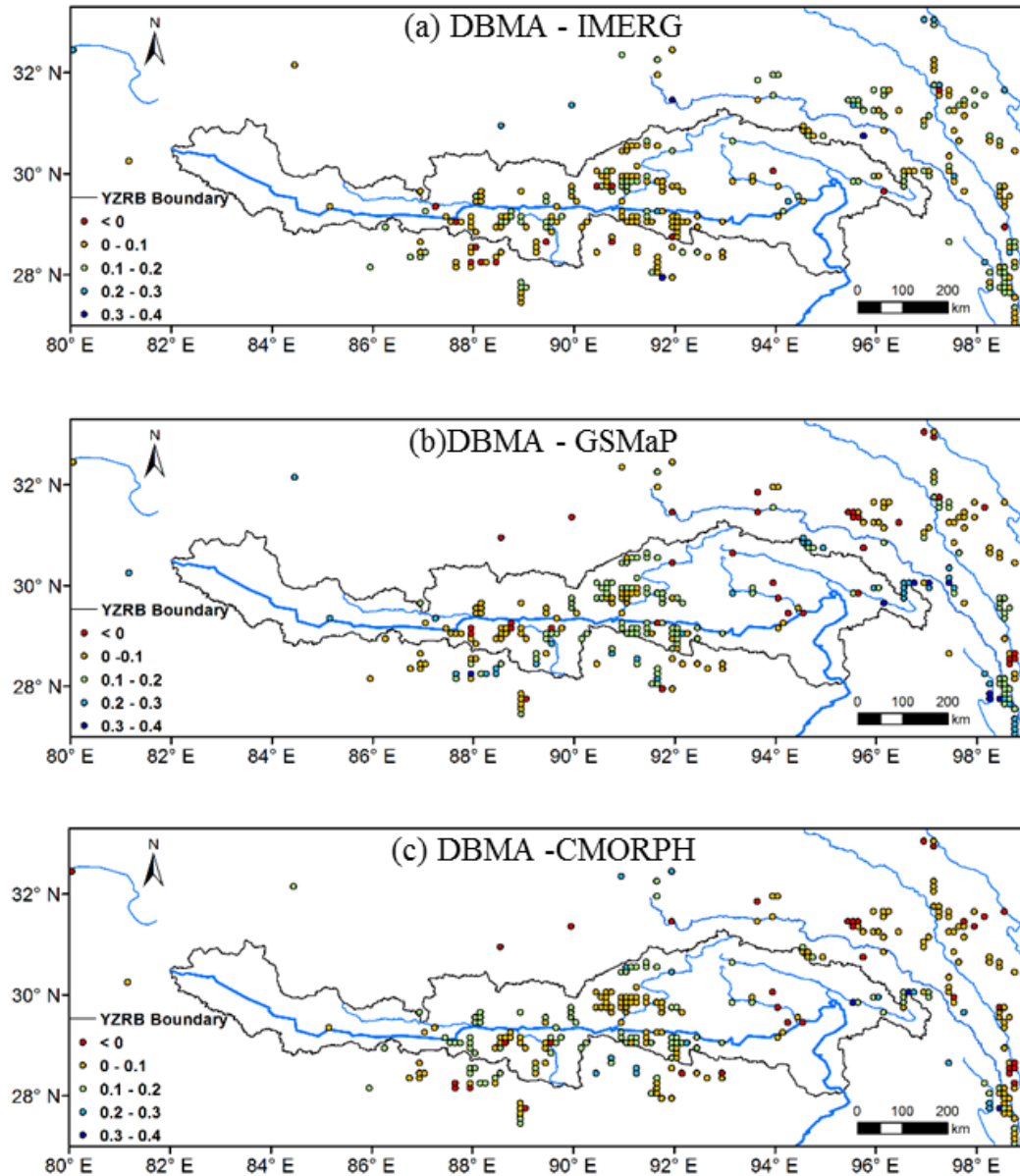
309   Figure 6. Spatial distributions of CC difference between (a) DBMA and IMERG, (b) DBMA and

310   GSMaP, (c) DBMA and CMORPH

311   **4.3. Hydrological Evaluation**

312   (a) Hydrological simulation

313   Performance of the THREW model forced by different rainfall datasets are

314   compared in Table 4. The DBMA-merged dataset achieved the best runoff simulation

315   among all rainfall inputs, with NSE reaching 0.93 and 0.86 in calibration and validation

316   period, respectively, indicating an excellent agreement between simulated and observed

317 hydrographs. Both IMERG and GSMaP underestimated the measured daily discharge,

318 but the DBMA-merged dataset improved such underestimations (see *RB* values in Table

319 5).

320 Table 5. Evaluation metrics of hydrological simulations forced by IMERG, GSMaP, CMORPH

321 and DBMA.

Parameters	IMERG	GSMaP	CMORPH	DBMA
NSEcal	0.91	0.90	0.90	0.93
NSEval	0.75	0.57	0.81	0.86
RB	-0.07	-0.10	0.02	-0.05

322 (b) Uncertainty analysis

323 The automatic algorithm pySOT was ran 200 times to investigate the modelling

324 uncertainty caused by parameter calibration. Figure 7 presents the distributions of *NSE*

325 values estimated by the ensemble parameter sets of the merged and original rainfall

326 forces. It is shown that streamflow simulated by the DBMA data at the Nuxia station

327 presented higher NSEs and smaller uncertainty ranges than that simulated by the

328 original satellite datasets, indicating that streamflow simulations driven by the merged

329 dataset showed stronger robustness and were less affected by uncertainty of parameter

330 calibration.

331 In addition to the Nuxia hydrological station, model performance on simulating

332 streamflow at the interior hydrological stations of Yangcun, Nugesha, Gongbujiangda

333 and Lhasa (Figure 1) were evaluated in Figure 7. It shows that the IMERG forced

334 simulations presented poor NSE outliers lower than zero at the Lhasa station, in spite

335 of their good performance at the Yangcun and Nugesha stations; the GSMaP forced

336 simulations presented large uncertainty ranges in calibration period at Nugesha and

337 Lhasa, and in validation period at Nuxia and Gongbujiangda; the CMORPH forced

338 simulations showed the worst performance in validation period at the interior

339 hydrological stations, despite their sound good performance in calibration period at

340 Yangcun and Nugesha. In comparison to the satellite datasets, the DBMA forced

341 simulations tend to perform consistently better with smaller uncertainties at all the

342 hydrological stations, which can be attributed to that the merged data incorporated the

343 advantages of different datasets in different regions and temporal periods and thus

344 better captured the spatial variability of rainfall inputs in sub-basins.
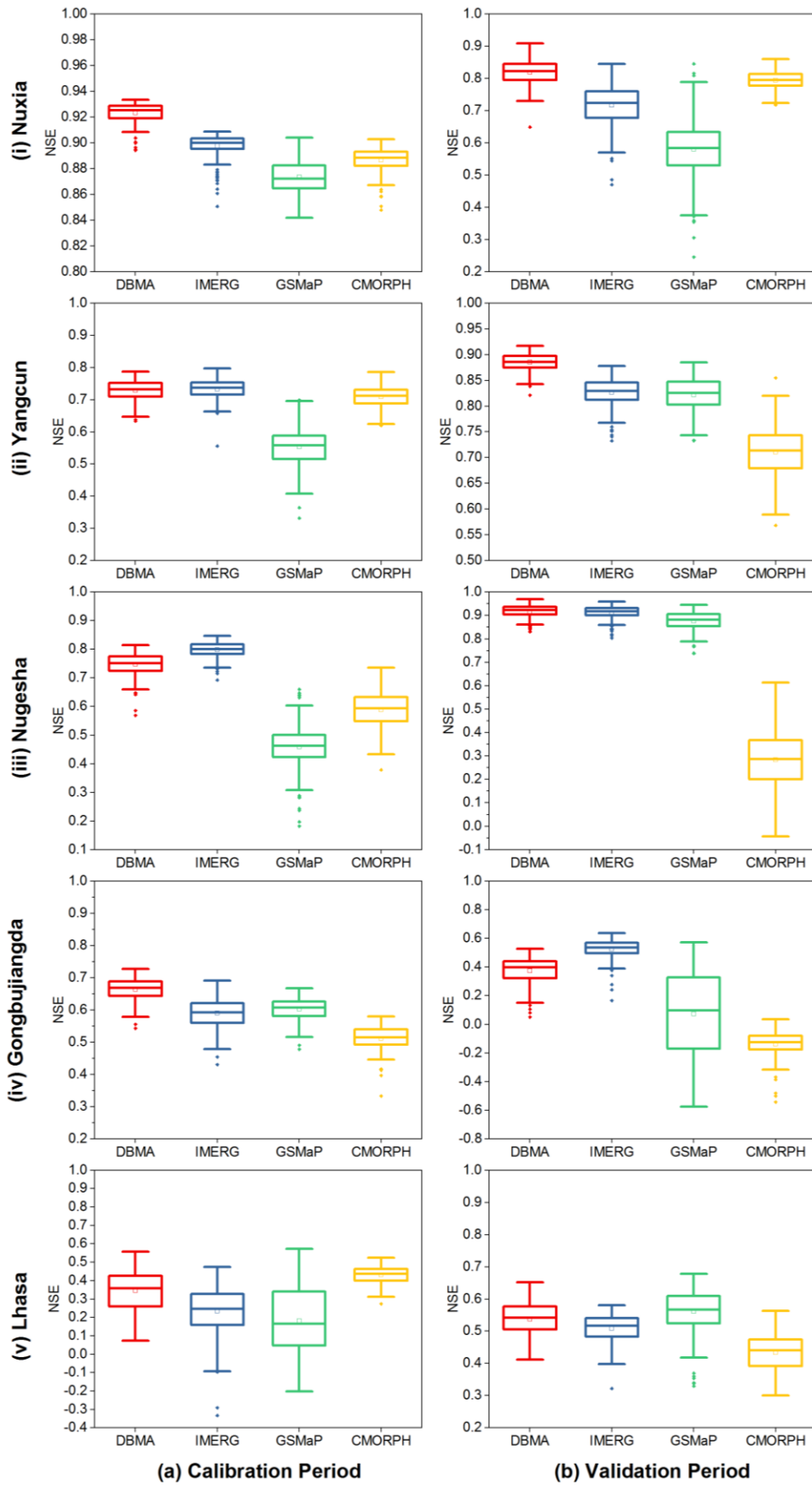
345 Figure 7. Runoff simulations at Nuxia, Yangcun, Nugesha, Gongbujiangda and Lhasa stations

347 forced by multiple rainfall inputs.

348 **4.4. Comparisons with other datasets**

349   To avoid interference of ground gauge data that merged in the DBMA dataset, the

350 ETC method introduced in Section 3.2 was applied to compare the three merged

351 datasets in Table 6. The RMSE and CC of DBMA calculated by ETC were 1.11 and

352 0.80, respectively, both of which are obviously superior compared to the corresponding

353 values estimated by CHIRPS and MSWEP, indicating that DBMA data is closer to the

354 true value of rainfall in the study region.

355   Table 6. Statistical RMSE and CC of merged datasets calculated by the ETC method.

Datasets	DBMA	CHIRPS	MSWEP
RMSE-ETC	1.11	7.15	2.82
CC-ETC	0.80	0.28	0.62

356   Runoff simulations forced by the three merged datasets during June 10th 2014 to

357 October 31st 2019 estimated by the corresponding optimal parameter sets were

358 presented in Figure 8. Note that the daily runoff is normalized as Eq. 8 for data security

359 reasons. Simulation by the CHIRPS data presented the lowest performance with NSE

360 values of 0.75 and 0.78 in the calibration and validation periods, respectively. The

361 DBMA forced simulation showed the highest performance with NSE values of 0.93

362 and 0.86 in the calibration and validation periods, followed by the MSWEP forced

363 simulation which estimated NSE values of 0.9 in the calibration period and 0.76 in the

364 validation period. The performance of streamflow forced by the merged datasets are

365 consistent with the agreements between the merged rainfall estimates and ground truth

366 shown in Table 6.

$$Q_{Normalized}^n = \frac{Q_{sim}^n - \min(Q_{obs})}{\max(Q_{obs}) - min(Q_{obs})} \tag{8}$$

367
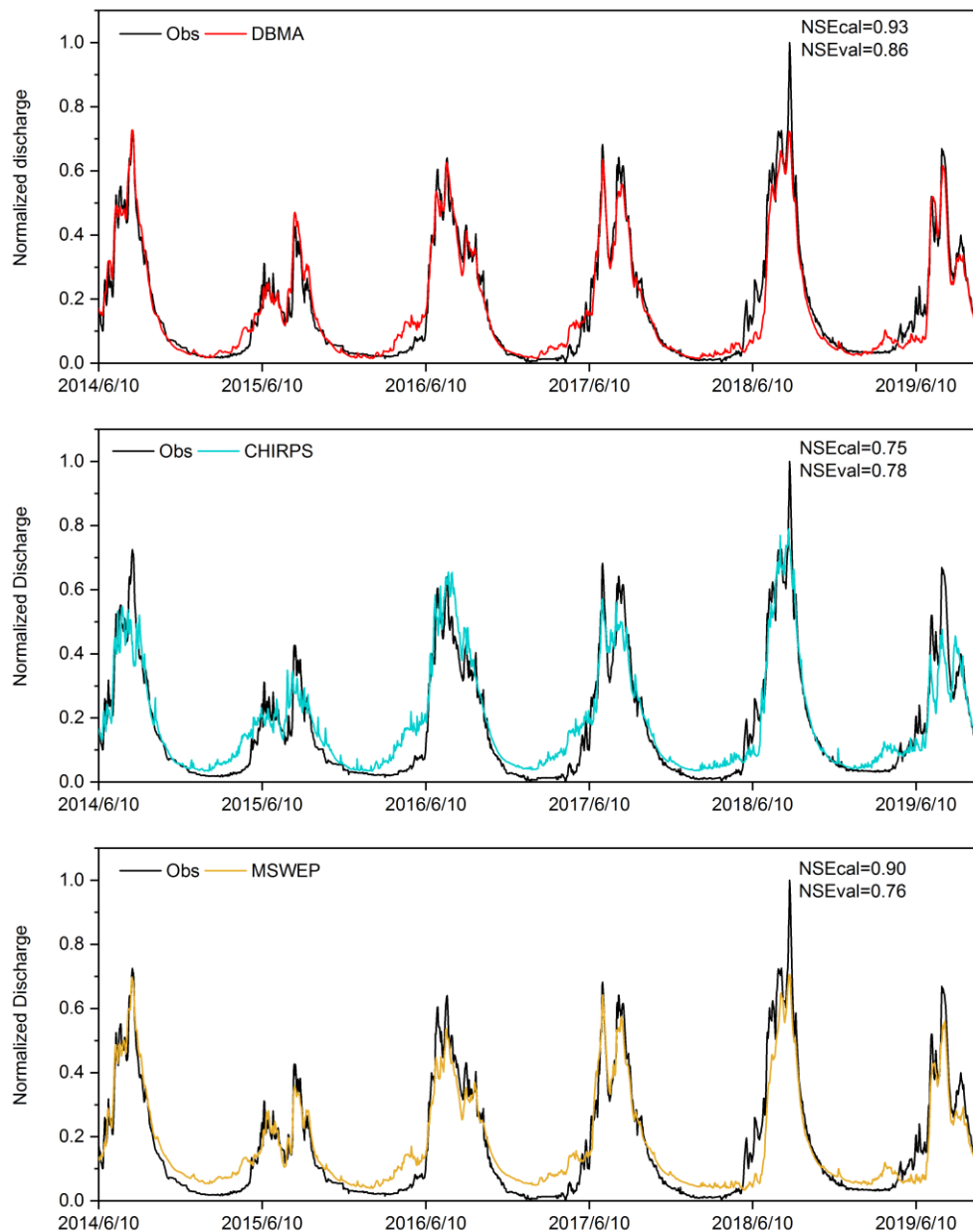
368   Figure 8. Simulated daily runoff at Nuxia station forced by DBMA, CHIRPS, and MSWEP.

369   **5 Data Availability**

370   The high-accuracy rain dataset by merging multi-satellite and dense ground

371   gauges over southern Tibetan Plateau for the warm seasons in 2014-2019 is freely

372   accessible   at   the   National   Tibetan   Plateau   Data   Center

373   https://doi.org/10.11888/Hydro.tpdc.271303 (Li et al.,2021).

6. Summary

We collated ground-based rainfall observations from a dense gauge network over southern TP. The gauged data provides crucial ground references of measured rainfall. Based on this rain gauge network and three satellite rainfall datasets of IMERG, GSMaP, and CMORPH, a merged rainfall dataset in six warm seasons from June 10th to October 31st during 2014-2019 over the southern TP was established. The DBMA method was used to estimate weights varying in space and time of the three satellite datasets for the merged data. The merged rainfall dataset presented improved performance on representing the total amount of rainfall and detecting the occurrence of gauged rainfall events, and provide a more reliable forcing for hydrological simulations in the YZRB, compared to the original satellite datasets. Comparisons with previous merged rainfall datasets of CHIRPS v2.0 and MSWEP v2 that used relatively sparse rain gauges in the study area demonstrated high values of the newly installed rain gauges for providing robust ground reference for the merging of current satellite datasets. Our results indicated that the merged datasets can meet the critical needs of accurate forcing inputs for the simulations of warm season floods and the robustness calibration of hydrological models. Based on this high-accuracy rainfall data and reliable hydrological modelling, much further research in this region then could be conducted, for example, fluvial sediment transport modelling through coupling sediment and hydrology, validation and correction of precipitation from Global Climate Model, and future runoff projections based on reliable modelling calibration in history.

Author contribution

TF and LK designed the research. LK, XR, MY developed the approach and datasets. LK downloaded the datasets and performed most of the computation and analysis work. YL, HZ, LH and MY contributed to the revising of the paper.

Competing interests

The authors declare that they have no conflict of interest.

Acknowledgements

Ground gauge data from the hydrological bureau of MWR is acknowledged here.

Financial support

This research has been financially supported by the National Natural Science Foundation of China (grant no. 92047301) and National Key R&D Program of China (2018YFC1508102).

References

Anagnostou, E. N., & Zhang, X.: Evaluation of Numerical Weather Model–Based Satellite Precipitation Adjustment in Tropical Mountainous Regions, Journal of Hydrometeorology, 20(3), 431-445, http://doi.org/10.1175/JHM-D-18-0008.1, 2019.

Beck, H. E., Wood, E. F., Pan, M., Fisher, C. K., Miralles, D. G., van Dijk, A. I. J. M., Adler, R. F.: MSWEP V2 Global 3-Hourly 0.1° Precipitation: Methodology and Quantitative Assessment, Bulletin of the American Meteorological Society, 100(3), 473-500, http://doi.org/10.1175/bams-d-17-0138.1, 2019.

Becker, A., Finger, P., Meyer-Christoffer, A., Rudolf, B., Schamm, K., Schneider, U., & Ziese, M.: A description of the global land-surface precipitation data products of the Global Precipitation Climatology Centre with sample applications including centennial (trend) analysis from 1901–present, Earth System Science Data, 5(1),

71-99, http://doi.org/10.5194/essd-5-71-2013, 2013.

Biskop, S., Maussion, F., Krause, P., & Fink, M.: Differences in the water-balance components of four lakes in the southern-central Tibetan Plateau, Hydrology and Earth System Sciences, 20(1), 209-225, http://doi.org/10.5194/hess-20-209-2016, 2016.

Bitew, M. M., & Gebremichael, M.: Evaluation through independent measurements: Complex terrain and humid tropical region in Ethiopia, Satellite rainfall applications for surface hydrology (pp. 205-214), Springer, Dordrecht, http://doi.org/ 10.1007/978-90-481-2915-7_12, 2010.

Bookhagen, B., & Burbank, D. W.: Topography, relief, and TRMM-derived rainfall variations along the Himalaya, Geophysical Research Letters, 33(8), http://doi.org/10.1029/2006gl026037, 2006.

David Eriksson, David Bindel, Christine A. Shoemaker.: pySOT and POAP: An event-driven asynchronous framework for surrogate optimization. *arXiv* preprint arXiv:1908.00420, 2019.

Derin, Y., Anagnostou, E., Anagnostou, M. N., Kalogiros, J., Casella, D., Marra, A. C., Sano, P.: Passive Microwave Rainfall Error Analysis Using High-Resolution X-Band Dual-Polarization Radar Observations in Complex Terrain, IEEE Transactions on Geoscience and Remote Sensing, 56(5), 2565-2586, http://doi.org/10.1109/tgrs.2017.2763622, 2018.

Derin, Y., Anagnostou, E., Berne, A., Borga, M., Boudevillain, B., Buytaert, W., Yilmaz, K.: Evaluation of GPM-era Global Satellite Precipitation Products over Multiple Complex Terrain Regions, Remote Sensing, 11(24), http://doi.org/10.3390/rs11242936, 2019.

Dinku, T. C., Stephen J.; Ceccato, Pietro.: Comparison of CMORPH and TRMM-3B42 over mountainous regions of Africa and South America, Satellite rainfall applications for surface hydrology (pp. 193-204): Springer, Dordrecht, http://doi.org/ 10.1007/978-90-481-2915-7_11, 2010.

448 Funk, C., Peterson, P., Landsfeld, M., Pedreros, D., Verdin, J., Shukla, S., Michaelsen,

449   J.: The climate hazards infrared precipitation with stations--a new environmental

450   record for monitoring extremes, Scientific Data, 2, 150066,

451   http://doi.org/10.1038/sdata.2015.66, 2015.

452 Gao, Y. C., & Liu, M. F.: Evaluation of high-resolution satellite precipitation products

453   using rain gauge observations over the Tibetan Plateau, Hydrology and Earth

454   System Sciences, 17(2), 837-849, http://doi.org/10.5194/hess-17-837-2013, 2013.

455 Goswami, D. C.: Brahmaputra River, Assam, India: Physiography, basin denudation,

456   and channel aggradation, Water Resources Research, 21(7), 959-978,

457   http://doi.org/ 10.1029/WR021i007p00959, 1985.

458 He, J., Yang, K., Tang, W., Lu, H., Qin, J., Chen, Y., & Li, X.: The first high-resolution

459   meteorological forcing dataset for land process studies over China, Scientific data,

460   7(1), 1-11, http://doi.org/ 10.1038/s41597-020-0369-y, 2020.

461 He, Z., Yang, L., Tian, F., Ni, G., Hou, A., & Lu, H.: Intercomparisons of Rainfall

462   Estimates from TRMM and GPM Multisatellite Products over the Upper Mekong

463   River Basin, Journal of Hydrometeorology, 18(2), 413-430,

464   http://doi.org/10.1175/jhm-d-16-0198.1, 2017.

465 Hong, Y., Gochis, D., Cheng, J.-t., Hsu, K.-l., & Sorooshian, S.: Evaluation of

466   PERSIANN-CCS Rainfall Measurement Using the NAME Event Rain Gauge

467   Network, Journal of Hydrometeorology, 8(3), 469-482,

468   http://doi.org/10.1175/jhm574.1, 2007.

469 Hou, A. Y., Kakar, R. K., Neeck, S., Azarbarzin, A. A., Kummerow, C. D., Kojima, M.,

470   Iguchi, T.: The Global Precipitation Measurement Mission, Bulletin of the

471   American Meteorological Society, 95(5), 701-722, http://doi.org/10.1175/bams-d-

472   13-00164.1, 2014.

473 Hou, S., Tian, F., Yang, L., Hu, H., & Hou, A.: How Does the Evaluation of the GPM

474   IMERG Rainfall Product Depend on Gauge Density and Rainfall Intensity?

475   Journal of Hydrometeorology, 19(2), 339-349, http://doi.org/10.1175/jhm-d-17-

476   0161.1, 2018.

477   Huang, J., Kang, S., Zhang, Q., Jenkins, M. G., Guo, J., Zhang, G., & Wang, K.: Spatial
478   distribution and magnification processes of mercury in snow from high-elevation
479   glaciers in the Tibetan Plateau, Atmospheric Environment, 46, 140-146,
480   http://doi.org/10.1016/j.atmosenv.2011.10.008, 2012.

481   Immerzeel, W. W., Van Beek, L. P., & Bierkens, M. F.: Climate change will affect the
482   Asian water towers, Science, 328(5984), 1382-1385, http://doi.org/
483   10.1126/science.1183188, 2010.

484   Jiang, S., Ren, L., Hong, Y., Yong, B., Yang, X., Yuan, F., & Ma, M.: Comprehensive
485   evaluation of multi-satellite precipitation products with a dense rain gauge
486   network and optimally merging their simulated hydrological flows using the
487   Bayesian model averaging method, Journal of Hydrology, 452-453, 213-225,
488   http://doi.org/10.1016/j.jhydrol.2012.05.055, 2012.

489   Joyce, R. J., JE; Arkin, PA; Xie, PP.: CMORPH: A Method that Produces Global
490   Precipitation Estimates from Passive Microwave and Infrared Data at High Spatial
491   and Temporal Resolution, Journal of Hydrometeorology, 5(3), 487-503, 2004.

492   Kidd, C., & Levizzani, V.: Status of satellite precipitation retrievals, Hydrology and
493   Earth System Sciences, 15(4), 1109-1116, http://doi.org/10.5194/hess-15-1109-
494   2011, 2011.

495   Kumar, V., Jain, S. K., & Singh, Y.: Analysis of long-term rainfall trends in India.
496   Hydrological Sciences Journal, 55(4), 484-496,
497   http://doi.org/10.1080/02626667.2010.481373, 2010.

498   Liu, J., Shangguan, D., Liu, S., Ding, Y., Wang, S., & Wang, X.: Evaluation and
499   comparison of CHIRPS and MSWEP daily-precipitation products in the Qinghai-
500   Tibet Plateau during the period of 1981–2015, Atmospheric Research, 230,
501   http://doi.org/ 10.1016/j.atmosres.2019.104634, 2019.

502   Lu, D., & Yong, B.: Evaluation and Hydrological Utility of the Latest GPM IMERG
503   V5 and GSMaP V7 Precipitation Products over the Tibetan Plateau, Remote

504   Sensing, 10(12), http://doi.org/10.3390/rs10122022, 2018.

505 Ma, Y., Hong, Y., Chen, Y., Yang, Y., Tang, G., Yao, Y., Liu, R.: Performance of
506   Optimally Merged Multisatellite Precipitation Products Using the Dynamic
507   Bayesian Model Averaging Scheme Over the Tibetan Plateau, Journal of
508   Geophysical Research: Atmospheres, 123(2), 814-834,
509   http://doi.org/10.1002/2017jd026648, 2018.

510 McColl, K. A., Vogelzang, J., Konings, A. G., Entekhabi, D., Piles, M., & Stoffelen, A.:
511   Extended triple collocation: Estimating errors and correlation coefficients with
512   respect to an unknown target, Geophysical Research Letters, 41(17), 6229-6236,
513   http://doi.org/10.1002/2014gl061322, 2014.

514 Nash, J. E. and Sutcliffe, J. V.: River flow forecasting through conceptual models part
515   I – A discussion of principles, Journal of hydrology, 10, 282–290,
516   https://doi.org/10.1016/0022-1694(70)90255-6, 1970.

517 Parsons, D. B., Rasmussen, R. M., Dai, A., & Trenberth, K. E.: The Changing Character
518   of Precipitation, Bulletin of the American Meteorological Society, 84(9), 1205-
519   1218, http://doi.org/10.1175/bams-84-9-1205, 2003.

520 Ren, Z. H., Zhao, P., Zhang, Q., Zhang, Z. F., Cao, L. J., Yang, Y. R., & Chen, Z.:
521   Quality control procedures for hourly precipitation data from automatic weather
522   stations in China, Meteorol. Mon, 36(7), 123-132, 2010.

523 Roebeling, R. A., Wolters, E. L. A., Meirink, J. F., & Leijnse, H.: Triple Collocation of
524   Summer Precipitation Retrievals from SEVIRI over Europe with Gridded Rain
525   Gauge and Weather Radar Data, Journal of Hydrometeorology, 13(5), 1552-1566,
526   http://doi.org/10.1175/jhm-d-11-089.1, 2012.

527 Stoffelen, A.: Toward the true near-surface wind speed: Error modeling and calibration
528   using triple collocation, Journal of Geophysical Research: Oceans, 103(C4), 7755-
529   7766, http://doi.org/10.1029/97jc03180, 1998

530 Su, Y., Zhao, C., Wang, Y., & Ma, Z.: Spatiotemporal Variations of Precipitation in
531   China Using Surface Gauge Observations from 1961 to 2016, Atmosphere, 11(3),

532   http://doi.org/10.3390/atmos11030303, 2020.

533   Sun, R., Yuan, H., Liu, X., & Jiang, X.: Evaluation of the latest satellite–gauge

534   precipitation products and their hydrologic applications over the Huaihe River

535   basin, Journal of Hydrology, 536, 302-319,

536   http://doi.org/10.1016/j.jhydrol.2016.02.054, 2016.

537   Tang, G., Ma, Y., Long, D., Zhong, L., & Hong, Y.: Evaluation of GPM Day-1 IMERG

538   and TMPA Version-7 legacy products over Mainland China at multiple

539   spatiotemporal scales, Journal of Hydrology, 533, 152-167,

540   http://doi.org/10.1016/j.jhydrol.2015.12.008, 2016.

541   Tang, G., Clark, M. P., Papalexiou, S. M., Ma, Z., & Hong, Y.: Have satellite

542   precipitation products improved over last two decades? A comprehensive

543   comparison of GPM IMERG with nine satellite and reanalysis datasets, Remote

544   Sensing of Environment, 240, http://doi.org/10.1016/j.rse.2020.111697, 2020.

545   Tong, K., Su, F., Yang, D., & Hao, Z.: Evaluation of satellite precipitation retrievals and

546   their potential utilities in hydrologic modeling over the Tibetan Plateau, Journal of

547   Hydrology, 519, 423-437, http://doi.org/10.1016/j.jhydrol.2014.07.044, 2014.

548   Tian, F., Hu, H., Lei, Z., & Sivapalan, M.: Extension of the Representative Elementary

549   Watershed approach for cold regions via explicit treatment of energy related

550   processes, Hydrology and Earth System Sciences, 10(5), 619-644, http://doi.org/

551   10.5194/hess-10-619-2006, 2006.

552   Ushio, T., Sasashige, K., Kubota, T., Shige, S., Okamoto, K. i., Aonashi, K., Kawasaki,

553   Z.-I.: A Kalman Filter Approach to the Global Satellite Mapping of Precipitation

554   (GSMaP) from Combined Passive Microwave and Infrared Radiometric Data,

555   Journal of the Meteorological Society of Japan, 87A, 137-151,

556   http://doi.org/10.2151/jmsj.87A.137, 2009.

557   Wang, Y., Wang, L., Li, X., Zhou, J., & Hu, Z.: An integration of gauge, satellite, and

558   reanalysis precipitation datasets for the largest river basin of the Tibetan Plateau.

559   Earth System Science Data, 12(3), 1789-1803, http://doi.org/10.5194/essd-12-

560   1789-2020, 2020.

561 Wang, Z., Zhong, R., Lai, C., & Chen, J.: Evaluation of the GPM IMERG satellite-
562   based precipitation products and the hydrological utility, Atmospheric Research,
563   196, 151-163, http://doi.org/10.1016/j.atmosres.2017.06.020, 2017.

564 Wilks, D. S.: Statistical methods in the atmospheric sciences (Vol. 100). Academic press,
565   2011.

566 Wolff, D. B., Nelkin, E. J., Bolvin, D. T., Huffman, G. J., Adler, R. F., Gu, G., Stocker,
567   E. F.: The TRMM Multisatellite Precipitation Analysis (TMPA): Quasi-Global,
568   Multiyear, Combined-Sensor Precipitation Estimates at Fine Scales, Journal of
569   Hydrometeorology, 8(1), 38-55, http://doi.org/10.1175/jhm560.1, 2007.

570 Xu, R., Tian, F., Yang, L., Hu, H., Lu, H., & Hou, A.: Ground validation of GPM
571   IMERG and TRMM 3B42V7 rainfall products over southern Tibetan Plateau
572   based on a high-density rain gauge network, Journal of Geophysical Research:
573   Atmospheres, 122(2), 910-924, http://doi.org/10.1002/2016jd025418, 2017.

574 Xue, X., Hong, Y., Limaye, A. S., Gourley, J. J., Huffman, G. J., Khan, S. I., Chen, S.:
575   Statistical and hydrological evaluation of TRMM-based Multi-satellite
576   Precipitation Analysis over the Wangchu Basin of Bhutan: Are the latest satellite
577   precipitation products 3B42V7 ready for use in ungauged basins? Journal of
578   Hydrology, 499, 91-99, http://doi.org/10.1016/j.jhydrol.2013.06.042, 2013.

579 Yang, D., Li, Z., Gao, B., Jiao, Y., Hong, Y., & Xu, T.: Multiscale Hydrologic
580   Applications of the Latest Satellite Precipitation Products in the Yangtze River
581   Basin using a Distributed Hydrologic Model, Journal of Hydrometeorology, 16(1),
582   407-426, http://doi.org/10.1175/jhm-d-14-0105.1, 2015

583 Yang, S., Chen, M., Xie, P., Yatagai, A., Hayasaka, T., Fukushima, Y., & Liu, C.: A
584   Gauge-Based Analysis of Daily Precipitation over East Asia, Journal of
585   Hydrometeorology, 8(3), 607-626, http://doi.org/10.1175/jhm583.1, 2007.

586 Yao, T., Thompson, L. G., Mosbrugger, V., Zhang, F., Ma, Y., Luo, T., & Fayziev, R.:
587   Third pole environment (TPE). Environmental Development, 3, 52-64, 2012

588 Yilmaz, K. K., Vergara, H. J., Rodríguez-Sánchez, J.-P., Salerno, F., Sahlu, D.,

589   Nikolopoulos, E. I., Derin, Y.: Multiregional Satellite Precipitation Products

590   Evaluation over Complex Terrain, Journal of Hydrometeorology, 17(6), 1817-

591   1836, http://doi.org/10.1175/jhm-d-15-0197.1, 2016.

592 Yong, B., Chen, B., Gourley, J. J., Ren, L., Hong, Y., Chen, X., Gong, L.:

593   Intercomparison of the Version-6 and Version-7 TMPA precipitation products over

594   high and low latitudes basins with independent gauge networks: Is the newer

595   version better in both real-time and post-real-time analysis for water resources and

596   hydrologic   extremes?   Journal   of   Hydrology,   508,   77-87,

597   http://doi.org/10.1016/j.jhydrol.2013.10.050, 2014.

598 Yong, B., Hong, Y., Ren, L.-L., Gourley, J. J., Huffman, G. J., Chen, X., Khan, S. I.:

599   Assessment of evolving TRMM-based multisatellite real-time precipitation

600   estimation methods and their impacts on hydrologic prediction in a high latitude

601   basin,   Journal   of   Geophysical   Research: Atmospheres,   117(D9),

602   http://doi.org/10.1029/2011jd017069, 2012.

603 Zhai, P., Zhang, X., Wan, H., & Pan, X.: Trends in total precipitation and frequency of

604   daily precipitation extremes over China. Journal of climate, 18(7), 1096-1108,

605   http://doi.org/ 10.1175/JCLI-3318.1, 2005.

606 Zhao, Y., Zhu, J., & Xu, Y.: Establishment and assessment of the grid precipitation

607   datasets in China for recent 50 years, J. Meteor. Sci, 34(4), 414-420, 2014.